Antagonistic effect of aspartate-β-hydroxylase on chemotherapeutics in cholangiocarcinoma

By

Kevin Y Cao

B.S., Indiana University, 2016

Thesis

Submitted in partial fulfillment of the requirements for the degree of Master of Science in the Department of Molecular Pharmacology, Physiology & Biotechnology at Brown University

PROVIDENCE, RHODE ISLAND

MAY 2019

AUTHORIZATION TO LEND AND REPRODUCE THESIS

As the sole author of the thesis, I authorize Brown University to lend it to other institutions or individuals for the purpose of scholarly research.

Date: _____ Signature: _____

Kevin Y Cao, Author

I further authorize Brown University to reproduce this thesis by photocopying or other means, in total or in part, at the request of other institutions or individuals for the purpose of scholarly research.

Date: _____ Signature: _____

Kevin Y Cao, Author

This thesis by Kevin Y Cao is accepted in its present form by the Department of Molecular Pharmacology, Physiology & Biotechnology as satisfying the thesis requirements for the degree of Master of Science.

Date: _____ Signature: _____

Jack R. Wands, Advisor

Date: _____ Signature: _____

Ji Su Li, Reader

Date: _____ Signature: _____

Chiung-Kuei Huang, Reader

Approved by the Graduate Council

Date: _____ Signature: _____

Andrew Campbell, PhD

Dean of the Graduate School

Acknowledgements

I would like to thank the Liver Research Center and all of its inhabitants for their help and support in this Master's training. In particular, I would like to say thanks to Dr. Wands for the opportunity to study under him, Rolf Carlson for lab management and making sure we have what we need, Chiung-Kuei Huang for the additional mentorship, guidance and opportunity to work alongside with, Ji Su Li for serving on my graduate committee and providing the criticism necessary to resolve unforeseen issues. This has been a long, tiring but educational journey filled with hard work, and the discovery of new knowledge.

Table of Contents

List of Figures

Background

Bile duct cancer, known as cholangiocarcinoma (CCA), is a rare but highly aggressive cancer with a 3% incident in all gastrointestinal cancers; in primary hepatic cancers, incidence is 10-30% [1, 2, 4]. The only known curative treatment for CCA is surgical resection at an early stage, however, CCA is usually asymptomatic until advanced local or metastatic stages where surgical resection may not be considered curative or possible therapy [2, 7, 9]. Clinical trials are being evaluated for treatment with a combination of two or more chemotherapeutic agents such as doxorubicin (DOX), 5-fluorouracil, cisplatin and gemcitabine (GCB) but results lack any significant difference in overall survival.

Cholangiocytes are the epithelial tissues of the bile duct. Their primary function is to control bile secretion and regulate bile flow. The hepatic bile duct capillaries are comprised of small cholangiocytes where as the main, or common, bile duct and tributaries are lined with large cholangiocytes. While these are the same type of cells, large cholangiocytes are more susceptible to damage, apoptosis, loss of function, and decreased

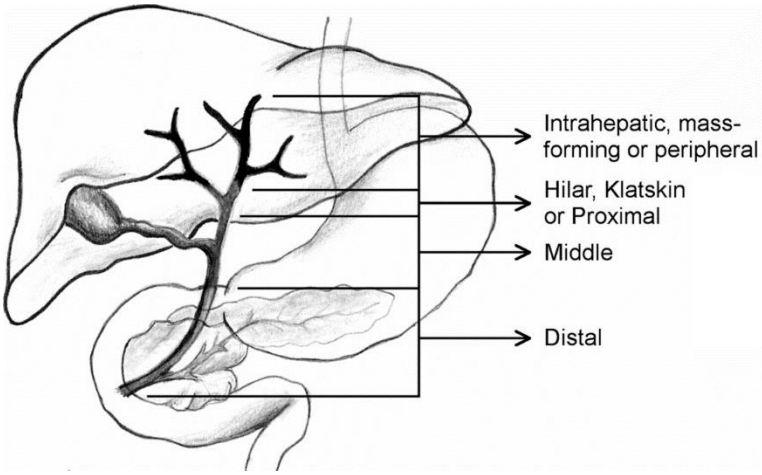

Figure 1. Anatomical distinction of bile ducts. CCA classification is based on the tissue of orgin. ICC arises from intrahepatic colagiocytes while all others forms of CCA are classified as ECC [5].

proliferation [3]. In fact, only 10% of CCA are intrahepatic cholagiocarcinomas (ICC). The majority of CCA occurs in common bile duct and categorized as extrahepatic cholangiocarcinoma (ECC) (Figure 1.) [5, 6, 8]. This disparity also reflects our understanding of the disease. While ECC research has made progress in the understanding of the disease and its mechanisms, as well as treatment options, there is limited understanding on the pathogenesis of ICC and effective therapies [2, 7].

ICC can be further classified based on its gene expression signature. An increase in cytokine expression and activation of STAT3 and inflammatory signaling pathways are properties of the inflammation class ICC [7. 8]. The proliferation class ICC is characterized by the activation of oncogenic signaling pathways, mutations, deletions, and copy number variants of genes, including KRAS and BRAF [7]. A comparison between inflammation and proliferation classes of ICC clearly highlights the greater severity of the proliferation class. Patients of the proliferation class ICC had shorter overall survival and time to recurrence (Figure 2) [7].

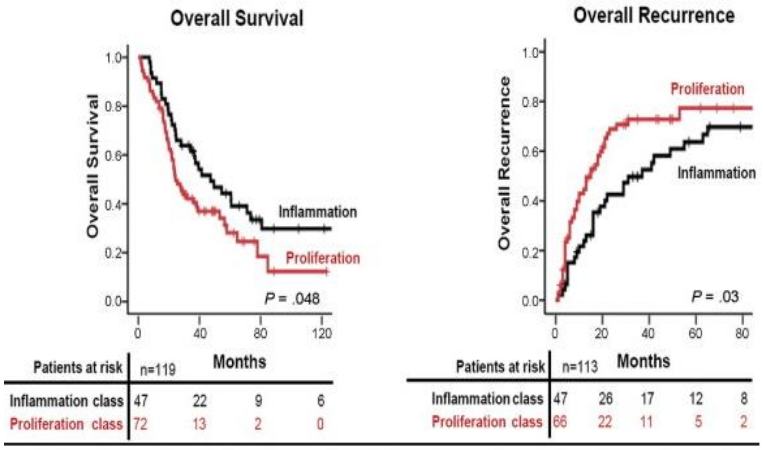

Figure 2. Inflammation and proliferation class in ICC prognosis. Kaplan-Meier plot highlights the differences in OS and recurrence between classes. Median survival was 24.3 months for proliferation class vs 47.2 months for inflammation class. Median time to recurrence also had proliferation class shorter at 15 months vs 37 months in the inflammation class [7].

Among altered genes, Aspartate-β-hydroxylase (ASPH), a type 2 transmembrane protein, is frequently found to be upregulated in primary hepatic cancers, including ICC of the proliferation class [7]. In fact, the prevalence of ASPH in ICC can be as high as 92%, with significant influence on tumor size, infiltration, aggression, and invasion. It has also been linked to poorer prognoses [10, 11].

Fe(II) and 2-oxoglutarate (2-OG) are co-substrates of 2-OG-dependent dioxygenases, which includes ASPH. These enzymes catalyze a myriad of oxygenation reactions such as protein modification, hydroxylation, demethylation, and DNA repair [12]. The function of ASPH is to catalyze the Asp and Asn residues in proteins with epidermal growth factor (EGF)–like domains and proteins within the notch1 family [13, 14, 15]. These hydroxylation targets are known cancer progression and metastasis mediators [16, 17, 18, 19]. In our previous studies in hepatocellular carcinoma (HCC), knockdown of ASPH substantially increased DNA damage, whereas overexpression of ASPH reduced it [24].

H2aX is nuclear protein that is essential to the DNA damage response. When a double stranded DNA break (DSB) occurs, H2aX is rapidly phosphorylated to γH2aX by a protein of the PI3k family which includes ATM, ATR and DNA-Pkcs. Along with the

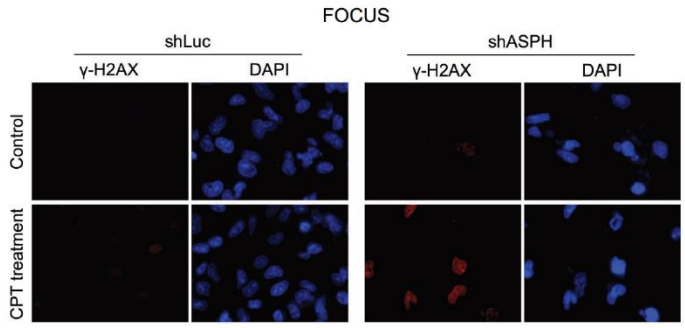

Figure 3. Immunofluorescence of γH2AX (red) and DNA (blue). Top row are challenged with DMSO as a control and camptothecin (CPT) in bottom rows [24].

phosphorylation of H2AX, these kinases also participate with γH2AX to recruit other members of DNA repair including the MRN complex [29]. This complex consists of 3 proteins, Mre11, Rad50 and Nbs1, and serves as a detector for DSB, a cell-cycle checkpoint, and the DSB repair mechanism. When the number of DSBs is too great, the expression of γH2aX will remain high, and the MRN complex can initiate apoptosis [25, 29]. This makes γH2aX a good biomarker that signifies the activation of the DNA repair mechanism meaning that an increase in γH2aX is indicative of an increase in DNA damage [20, 26, 29]. Iwagami et al. demonstrated challenging cells with a DNA damage

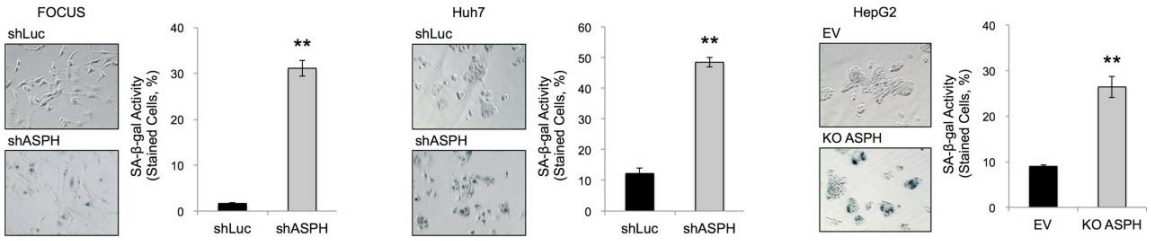

*Figure 4. Induced senescence in HCC. shRNA inhibition of ASPH stained with senescence-associated β-galactosidase (SA-β-Gal). Cells in senescence are stained blue. **P<0.01 [24].*

inducer, CPT, in knockdown ASPH cells induced γH2aX expression [24]. The physiological effects of an increase in γH2aX protein expression is an inhibition of growth, or induced senescence and apoptosis.

Senescence is a desirable outcome for cancer treatments as this would mean tumor proliferation has been halted. Senescence can be induced by one of many factors including truncation of telomeres, certain oncogene expressions, oxidative damage, chromosomal perturbations and DNA damage [21, 22]. However, these factors can also be oncogenic and tumors frequently have altered signaling pathways to bypass senescence and apoptosis [23]. Our previous study in HCC demonstrated that induced

senescence was possible by targeting ASPH. This was achieved using two methods; by targeting ASPH with a small molecule inhibitor (SMI), MO-I-1151 in conjunction with the chemotherapeutic agent DOX and by inhibiting ASPH expression with the use of short hairpin RNA (shRNA) (Figure 4) [24].

While HCC and CCA originate in close proximity to one another there are still numerous differences between them. In this study we sought to explore and expand the potential therapeutic target ASPH in a different cancer, CCA. Additionally, we aim to elucidate the mechanisms of ASPH with respect to DNA damage and the DNA repair mechanism.

Materials and Methods

Lentivirus production

HEK-293T cells were used to produce lentivirus by transfection with TransIT®-LT1 Reagent (Mirus Bio LLC, Madison, WI, USA). Lentivirus plasmids, pLKO.1-shRNA-luciferase and pLKO.1-shRNA-ASPH, were purchased from Sigma-Aldrich (St. Louis, MO, USA). The ASPH plasmid was constructed in house based off of PCDH.puro database. Viruses were produced using 15 μg of lentivirus plasmid, 8.5 μg of psPAX2 (containing GAG, POL) and 5 μg of pMD2.G (containing VSVg) in a 10 cm dish. Virus containing medium was collected after 48 hours and filtered through a 0.45 μm filter followed by infection of target cells.

Cell lines

H1 and HuccT1 cell lines were derived from intrahepatic cholangiocarcinoma. Cell lines were maintained in Roswell Park Memorial Institute medium supplemented with 10% fetal bovine serum, 2mM L-glutamine and 1% of Penicillin-Streptomycin solution in a humidified 37^{o}C incubator with 5% CO_2.

OUMS29 is an immortalized hepatocyte cell line and HEK-293T was derived from human embryonic kidney cells. These cell lines were maintained in Dulbecco's Modified Eagle Medium with the same supplements and incubator conditions as above.

Cytoplasmic and nuclear fraction extraction

Nuclear and cytoplasmic extraction was done using the NE-PER™ extraction kit (Thermo Fisher; 78833). Cells were detached using trypsin then centrifuged at 500 rpm to pellet. Medium was removed and cell pellet washed with PBS by centrifugation at 500 rpm. Once PBS was removed the cells were subject to nuclear and cytoplasmic extraction according to the manufacturer protocol. In brief, CER I was added to the pellet to resuspend cells by vortexing followed by incubation on ice for 10 minutes. CER II was then added and samples vortexed for 5 seconds on high, incubated on ice for 1 minute then vortexed again before centrifuged at 14000 rpm for 5 minutes. The supernatant containing the cytoplasmic fraction was removed and the pellet was resuspended using ice-cold NER. Solution was then vortexed for 15 seconds every 10 minutes for a total of 40 minutes then centrifuged at 14000 rpm for 10 minutes. Supernatant containing the nuclear fraction was removed immediately.

Protein lysate

Cells were washed with 7.4 pH PBS and lysed with RIPA buffer (Alfa Aesar; J62524) with addition of phosphate and phosphatase inhibitor (Thermo Fisher; 78428, 78430. Plates were shaken at 4^{o}C for 20 minutes then collected and centrifuged at 14,000 rpm for 15 minutes. Protein lysate was transferred to a new tube. Cell debris was discarded.

Animal tissues were cut then lysed using a 5mm tungsten bead (Qiagen: 69997) and shaken at 20 Hz for 3 minutes. Lysate was incubated on ice for 20 minutes then centrifuged at 14,000 rpm for 15 minutes. Protein lysate was transferred to a new tube. Cell debris was discarded. Tungsten bead was collected for reuse after it is autoclaved.

Protein concentration was measured by BCA assay (Thermo Fisher; 23225) per manufacturer protocol. Protein quantity was calculated based on $y = \frac{1x}{adj\ concentration}$ where x is the desired µg of protein, adj concentration is the adjusted measured absorbance of the sample, and y is the µl of sample for x µg of protein.

Protein lysates were added to protein sample buffer then denatured at 96°C for 5 minutes and rapidly cooled on ice for an additional 5 minutes for use in western blot.

Western blot analysis

Cell lysates were separated by SDS-PAGE at 80 V then wet transferred to a PVDF membrane at 100 V for 2 hours. Membrane was blocked with 5% milk for a minimum of 1 hour then incubated with appropriate primary antibody overnight at 4°C. HRP-conjugated secondary antibody in 2.5% milk were added and incubated for 1 hour followed by washing with 0.5% TBST for 10 minutes x 5 times.

Images were taken using SuperSignal West Dura Extended Duration Substrate (Thermo Fisher; 34075). Experiments were all triplicated, densitometric analysis was done using Image J (NIH).

Primary antibodies used and their source are listed below. Dilutions used were 1:1000 TBST unless otherwise specified.

Table 1. Antibodies used in Western blot

Antibody	Source
Polyclonal ASPH	In house
Myc	Cell Signaling #2276
HA	Santa Cruz sc-7392
α-tubulin 1:3000	Sigma Aldrich T5168
GAPDH 1:5000	Santa Cruz sc-32233
yH2aX	Cell Signaling #9718
ATM/ATR substrate	Cell Signaling #6966
Mre11	Cell Signaling #4895
ATM	Sigma Aldrich A1106
Rad50	Cell Signaling #3427
Nbs1	Cell Signaling #14956
H3	Cell Signaling #9715

Co-Immunoprecipitation

Protein lysates were subjected to IP with either HA or ATM antibody overnight at 4^{o}C. Normal mouse IgG (Santa Cruz, sc-2025) and normal rabbit IgG (Santa Cruz, sc-2027) were used as negative controls. Antibody probes were coupled to Protein A/G PLUS-Agarose (Santa Cruz, sc-2003) for 1 hour then washed with RIPA for 5 minutes and centrifuged at 3000 rpm for 2 minutes x 4 times. Supernatant was removed and protein sample buffer was added then heated to 96^{o}C for 5 minutes to detach and denature IP conjugate from agarose. Analysis was completed by Western Blot.

Cellular proliferation assay

Cell proliferation assay, or MTT was performed using 3-(4,5-dimethylthiazol-2-yl)-2,5-diphenyl-tetrazolium bromide (MTT; Sigma-Aldrich). Cells were seeded in 96 well plates at a concentration of $1x10^4$ to $3x10^4$ cells/ml. MTT powder was dissolved in

sterilized 7.4 pH PBS at a concentration of 5 mg/ml. MTT solution was mixed with medium at a ratio of 1:10 then added to the wells and incubated at 37^{o}C for 1 hour. MTT solution was then replaced with DMSO and cells shaken for 30 minutes at room temperature and read for absorbance at 465 nm wavelength.

Numbers of plates were determined by the number of time points to be collected, plus one for day 0 control. The experimental design dictates MTT to be done on days 0, 1, 3, 5, 7 or consecutive days 0, 1, 2, 3. Treatments and compounds were added the following day after seeding at day 0.

Soft agar colony formation assay

Cells were seeded at a density of 2.5 x 10^3 cells/well on a 6 well plate in complete medium containing 0.4% Noble agar (Sigma-Aldrich; A5431) and treatment compounds. This soft agar layer was laid over a 0.8% Noble agar containing medium and treatment compounds. Cells were grown for 21 days with medium change twice a week. Colonies after 21 days were stained with 10% Giemsa solution, counted and analyzed using Image J.

Senescence-associated β-galactosidase staining

Senescence was measured using a senescence detection kit (BioVision; K320-250) and conducted per manufacturer protocol. Cells were seeded at a density of 2x10^5cells/well then treated with DMSO or 5mM DOX in 12 well plates for 24 hours before staining with β- galactosidase. Number of blue stained cells and total cells were counted to determine the percentage of SA-β-gal activity. Quantification was performed

by taking 4 randomly selected microscope fields and averaging the number of cells that were stained blue.

Cell Viability Assay

Cells were seeded at a density of $1x10^5$ cells/well in a 6 well plate. Wells were treated with either DMSO or 0.5mM DOX for 3 days. The medium was then removed and washed with PBS then cells stained with crystal violet (Sigma-Aldrich) solution (0.5% crystal violet, 30% ethanol, 3% formaldehyde) and washed with PBS 5 times then dried. DMSO was added to dissolve crystal violet. Absorbance was measured at 550nm.

In vivo study

Eight week-old nu/nu nude mice (Charles River Laboratories, Wilmington, MA) were kept in a clean room and had access to standard food and sterilized water. H1 CCA cells ($2x10^6$) suspended in 50 µl of serum-free medium and 50 µl of Matrigel (Becton, Dickinson, Franklin Lakes, NJ) were injected into the liver parenchyma. After 4 days incubation, treatment began by intraperitoneal injection of MO-I-1151 twice a week at 25 mg/kg and DOX 3 times a week at 2mg/kg. Treatment continued for 3 full weeks then animals euthanized. Tumors dimensions were measured by calipers. Tumor volume was determined by the formula $V = \frac{(lw)^2}{2}$, where *l* is the combined length and *w* is the combined width of all tumors. Statistics were calculated using one-way ANOVA.

Eight week old rats (Charles River) were fed with a standard diet and given free access to water. shLuc or shASPH transfected BDE-NEU cells ($2x10^6$)suspended in 50 µl

of serum-free medium, and 50 µl of Matrigel were inoculated into the liver parenchyma. After 4 days incubation period, treatment started with an injection of DOX at 2mg/kg by intraperitoneal injection 3 times a week for a total of 18 days. The rats were then euthanized. Tumors were weighed. Statistics was done by student t test.

Results

ASPH upregulation suppressed DNA damage but its downregulation stimulates it.

To determine if ASPH is involved in chemotherapy associated DNA damages in CCA tumors, we used CCA cell lines SSP25 and HuCCT1, both are high in ASPH expression. If ASPH-mediated DNA damage is universal, knockdown of ASPH in these cell lines combined with chemotherapy should induce greater DNA damage than the control. Immunoblotting for ASPH in SSP25 and HuCCT1 depicted an increase in γH2aX protein expression when treated with chemotherapeutic agents Camptothecin (CPT) and DOX. γH2aX was further increase when cells were targeted with shRNA-ASPH (shASPH) to knockdown ASPH expression (Figure 5A, B). Ectopic expression of ASPH done in two different cell lines, OUMS29 and HEK-293T, with the same experimental conditions yielded a reduction in γH2aX expression when compared to WT cells treated with CPT (Figure 5C, D). This diminishing phenotype of γH2aX expression in the presence of ASPH was lost when cells were transfected with an enzymatically dead version of ASPH named $ASPH^{V3}$ (Figure 5E).

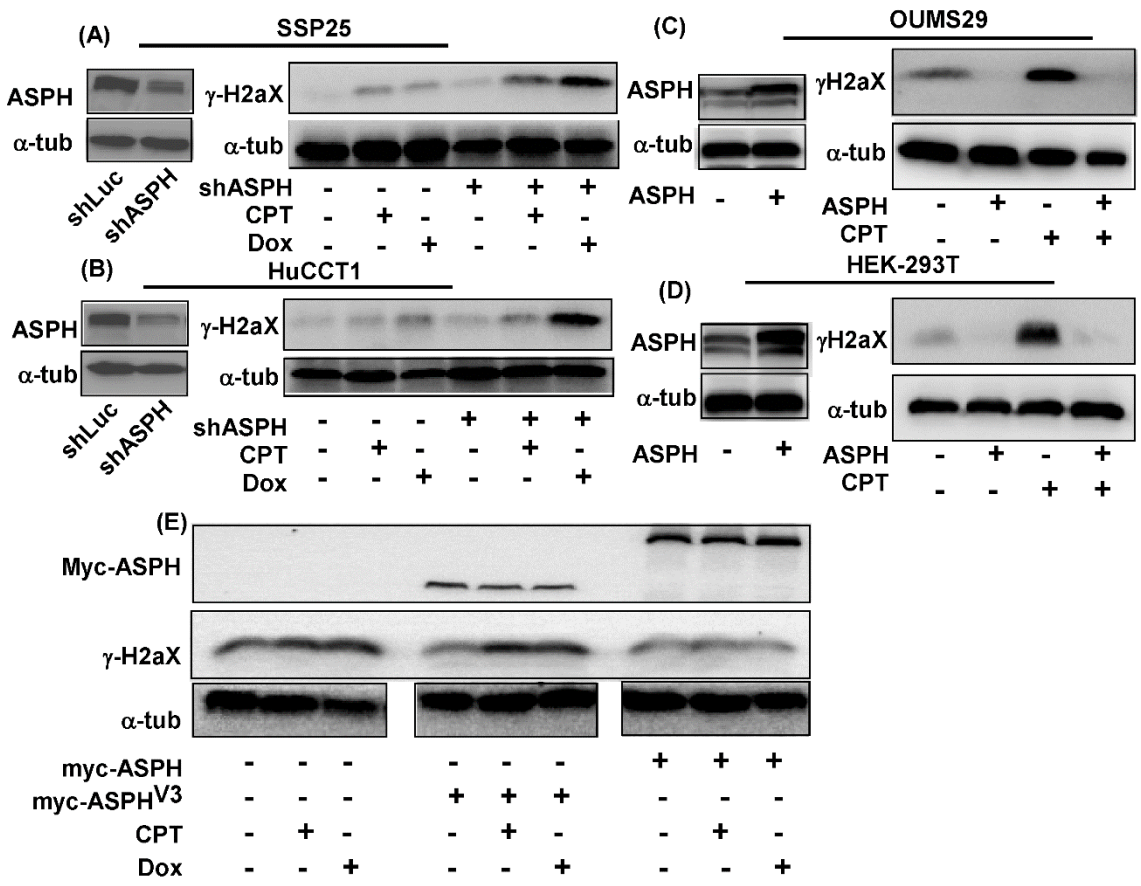

Figure 5. ASPH negatively regulates DNA damage. γH2aX expression was determined to quantify DNA damage in CCA cell lines (A) SSP25 and (B) Hucct1. ASPH was knocked down using shASPH with shLuc as a control. Cells were challenged with either 2.5uM DOX or 20uM CPT for 2 hours. γH2aX was also determined in (C) OUMS29 and (D) HEK-293T cells transfected with ASPH and challenged with the same conditions as in A and B. γH2aX expression was determined in two forms of ASPH, full length and variant 3, in (E) HEK-293T cells with the same conditions above. Variant 3 form lack the catalytic domain.

2-OG suppressed chemotherapeutic response

The effects of chemotherapy on DNA damage were reduced in the presence of ASPH and knockdown of ASPH enhanced it. The substrate 2-OG is believed to influence ASPH activity on its targets, including DNA damage. Thus, we treated HEK-293T cells with 2-OG to check whether it can alleviate the insufficient expression of ASPH in reducing DNA damage. HEK-293T was pretreated with increasing concentrations of 2-

OG then challenged with 20μM CPT for 2 hours before collecting the protein lysates and analyzing by western blot. ASPH was checked to confirm the transfection of ASPH with α-tubulin as an internal control. DNA damage was discovered to decrease with respect to an increase in 2-OG concentration. However, this effect is masked by ASPH when its expression was sufficient (Figure 6A). MTT assay using CCA cell line H1 pretreated with 2-OG then exposed to DOX demonstrated an improvement in growth rate with increasing concentrations of 2-OG compared to DMSO control (Figure 6B).

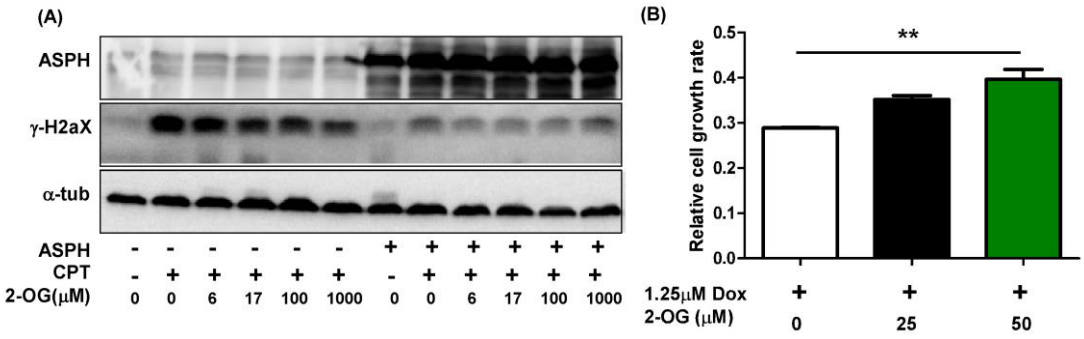

*Figure 6. 2-OG attenuates DNA damage from chemotherapy. (A) HEK-293T cells pretreated with increasing concentrations of 2-OG for 24hours then challenged with 20uM CPT for 2 hours. γH2aX expression was determined by western blot. Relative growth rate of (B) H1 cells in MMT assay with 0, 25 or 50 μM 2-OG addition in 1.25uM DOX at Day 2. **, p<0.01 by ANOVA analysis*

Knockdown of ASPH promoted chemotherapeutic response in CCA cells

To measure the antitumor effect of targeting ASPH in combination with chemotherapy, H1 cells were transduced with shLuc as a control or shASPH via a lentiviral system. Cell viability, MTT, soft agar colony formation, and senescence assays were performed in the transfected H1 cells. Cell viability using crystal violet demonstrated a significant decrease in the number of viable H1 cells in the well after exposure to 0.5uM DOX for 3 days. Quantification by absorbance revealed shASPH-H1

cells had poorer viability overall than shLu-H1 cells with shASPH-DOX inhibiting cell viability the greatest (Figure 7A). MTT assay challenged with 0.63uM DOX was measured at days 0, 1, 2, and 3. A similar conclusion resulted with shASPH-DOX having the greatest inhibition in cell proliferation with shLuc-DOX and shASPH-DMSO having partial effects in cell proliferation inhibition compared to shLuc-DMSO control (Figure 7B). Knockdown of ASPH significantly reduced colony formation in soft agar with the addition of 0.5uM DOX reducing colony count as well as colony size. As expected, the combination of shASPH-DOX had the fewest number of countable colonies as well as smaller colonies overall compared to control shLuc-DMSO (Figure 7C). The number of induced senescent cells after 24 hour exposure to 5uM DOX and staining with SA-β-gal was greater in shASPH-DOX compare to all other groups (Figure 7D). These findings suggest targeting ASPH in combination with chemotherapy has a synergistic effect in reducing cell proliferation in CCA as well. Additionally, any remaining cells as found in shASPH-DOX group in colony formation may not be viable cells or may be in an induced senescent state effectively halting tumor progression.

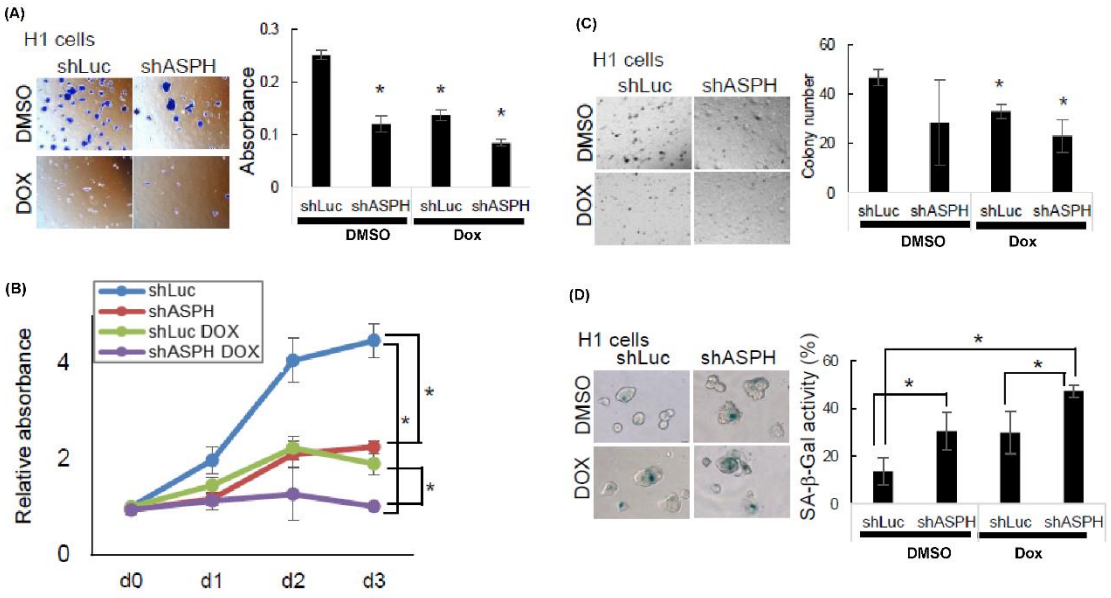

*Figure 7. Synergistic reduction in malignant progression in CCA cells by targeting ASPH and treatment with DOX. (A) Cell viability of shLuc-H1 control and shASPH-H1 challenged with DMSO or 0.5μM DOX for 3 days. Left panel: representative photographs of crystal violet staining (x200), Right panel: quantification of crystal violet staining (n=3). (B)Relative growth of shLuc-H1 control and shASPH-H1 challenged with DMSO or 0.63μM DOX for 3 consecutive days. (C) Left panel: Representative image of shLuc-H1 control and shASPH-H1 challenged with DMSO or 0.5μM DOX at 21 days in soft agar. Right panel: number of colonies quantification. (D) Left panel: representative image of senescence-associated (SA) b-gal staining in shLuc-H1 control and shASPH-H1 challenged with DMSO or 5μM DOX for 24 hours. Right panel: quantification of SA b-gal staining activity. *p<0.05.*

Synergistic anti-tumor effect of targeting ASPH and chemotherapy in vivo.

To evaluate the synergistic effects of ASPH and chemotherapy, two in vivo orthotropic xenograft models were established. BDE-NEU cells transfected with either shLuc or shASPH was inoculated into the rat liver parenchyma and treated with PBS as control or DOX 3 times a week for 18 days. In this rat model, mean tumor weight was significantly lower in shASPH-DOX group compared to PBS treated control and shASPH group. DOX treatment in shLuc group had an undesirable effect in mean tumor weight with an observed no change or increase in tumor weight (Figure 8A and B). The second

model using immunocompromised *nu/nu* nude mice were orthotopically inoculated with H1 cells. These H1-grenerated tumors were treated with ASPH inhibitor MO-I-1151, a second generation compound with improved solubility, binding affinity and enhanced ASPH inhibition compared to first generation MO-I-1100 [27, 28]. Additionally these mice were also treated with DOX. The combination of MO-I-1151 and DOX was given for 3 weeks every other day. Tumor size reported was based on volume calculations as described above. The combination of inhibiting ASPH and treating with DOX had the greatest effect in reducing total tumor volume compared to control and DOX treatment alone (Figure 8C and D).

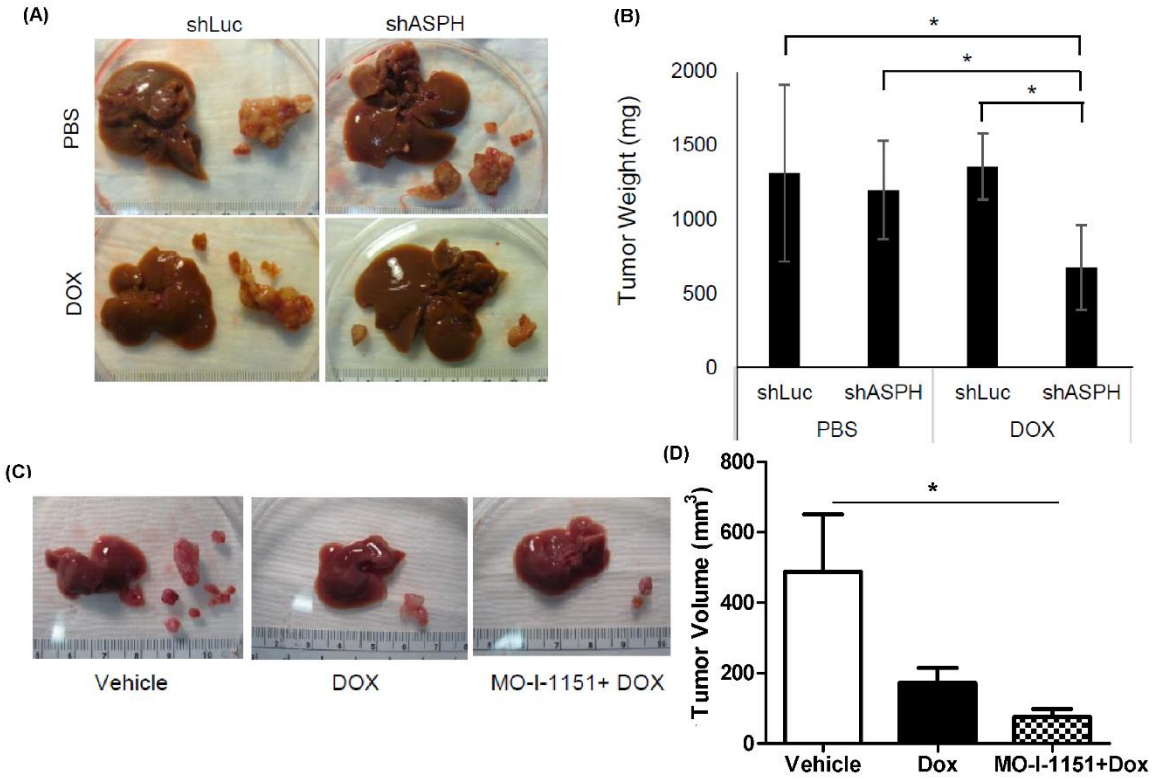

*Figure 8. Targeting ASPH in conjunction with chemotherapy synergistically reduce CCA progression in vivo. BDE-NEU rat CCA cells with transfected with shLuc or shASPH were inoculated into the rat's liver. Treatment was given at 2mg/kg Dox treatment 3 times per week for 18 days. (A) Representative image of rat liver and corresponding extracted tumors. (B) Quantification of tumor weight. *, p<0.05 by student t test. H1 CCA cells were inoculated into nude mice livers and treated with 25mg/kg ASPH SMI, MO-I-1151 (1151) every other day and/or 2mg/kg Dox 3 times per week for 3 weeks. (C) Representative image of nude mice liver and tumor morphology. (D) Quantification of total tumor volume, n=6-8. *, p<0.05 by one way ANOVA.*

ASPH interacted with ATM in DNA repair activity

The process of DNA repair involves the recruitment, activation and activity of a number of enzymes and substrates. We have shown in this study that ASPH reduced DNA damage in the presence of a DNA damage inducer (Figure 5). We evaluated the DNA repair pathway in HEK-293T cells transfected with EV or shASPH and challenged with CPT in a time course study. ASPH overexpression reduced ATM/ATR substrates but no significant changes to ATM and MRN expression (Figure 9A and B). Although ASPH is described as a type 2 transmembrane protein [13], ASPH seems to have influence on

DNA damage response (Figure 5). This infers its presence within the cell is not exclusive to the cell membrane and cytoplasm. A nuclear and cytoplasmic fraction extraction of HEK-293T cells reveals an increase in Nbs1 expression when treated with DOX but no change in the other proteins in the MRN complex. More importantly, ASPH was detected in both cytoplasm and nucleoplasm fractions (Figure 9C).

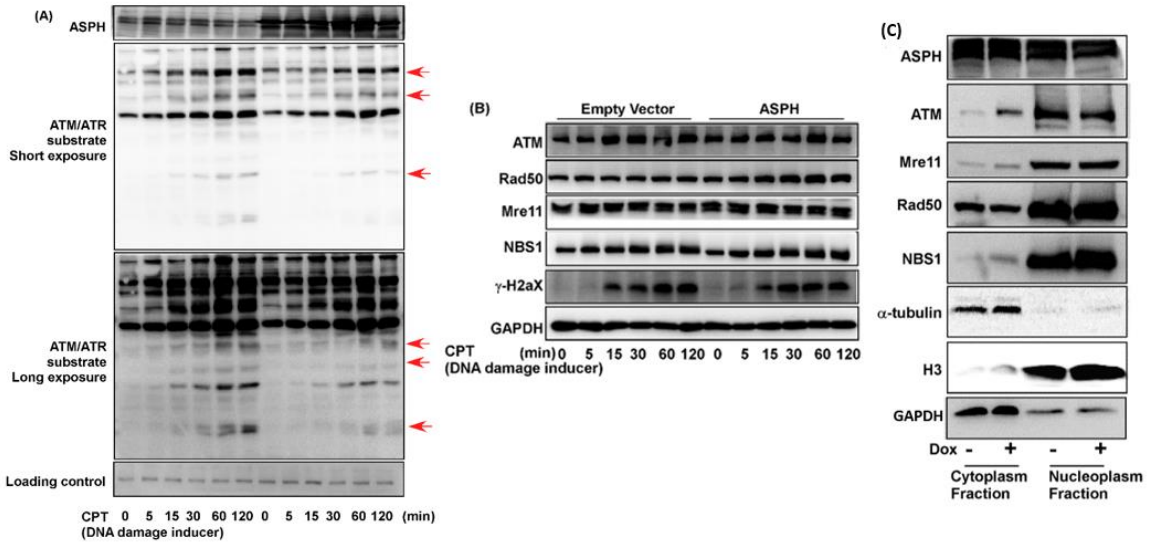

Figure 9. ATM expression in response to upregulation of ASPH. HEK-293T cells expressing EV or ASPH were challenged with 10μM CPT in a time course study. (A) Short and long exposure images of ATM/ATR substrates were shown. Red arrows indicate reduced ATM/ATR substrates in ASPH expressing HEK-293T cells. (B) ATM and MRN complex expression of HEK293T cells challenged with 10μM CPT. (C) Cytoplasm and nucleoplasm fractions of HEK-293T cells treated with or without DOX.

The presence of ASPH within the nucleus or nuclear membrane suggests potential involvement with DNA damage response. Immunoprecipitation using anti-HA demonstrated ASPH had binding to ATM. The MRN complex is a known interactor with ATM thus detectable in both cytoplasmic and nuclear fractions (Figure 9C). Pull down using anti-ATM was able to confirm this finding. ATM has physical interactions with ASPH and the MRN complex (Figure 10A and B). Furthermore, challenging transfected HEK-293T cells with DOX in an ATM pulldown revealed an increase in binding to NBS1 in

ASPH overexpressed cells compared to EV control. DMSO controls lacked induced DNA damage thus had significantly lower ATM expression and subsequently MRN binding (Figure 10C).

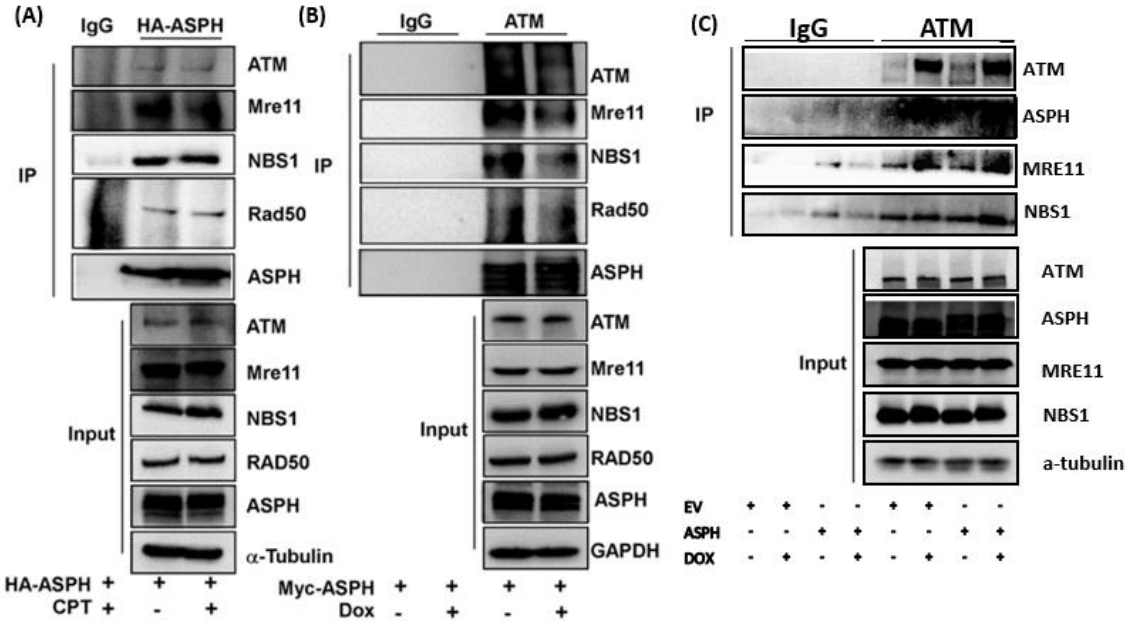

Figure 10. ASPH binds to ATM and the MRN complex. (A) HEK-293T expressing HA tagged ASPH was treated with 10μM CPT for 1 hour. Protein lysate was collected for IP and pulled down using HA antibody with IgG as the control. ATM and MRN complex was observed to bind to ASPH. (B) Myc-ASPH expressing HEK-293T cells were challenged with 2.5μM DOX for 2 hours. Protein lysates were collected for IP and pulled down using ATM antibody with IgG as the control. ASPH was observed to bind to ATM. (C) HEK-293T cells expressing EV or ASPH was challenged with either DMSO or 2.5μM DOX for 2 hours. Protein lysates were collected for IP and pulled down using ATM antibody with IgG as a control. DOX treated conditions has abundant ATM pulldown in comparison to DMSO groups. NBS1 binding to ATM is increased in elevated levels of ASPH.

Discussion

During embryonic development the expression of ASPH is necessary for proper development of the eyes and facial structures [32], however the expression of ASPH in adult tissue is very low or negligible [33]. In cancer, ASPH re-emerges and has been found to be up regulated in multiple types of cancers, including CCA [24, 27, 28, 30, 31]. ASPH has been shown to promote a malignant phenotype when overexpressed and the targeting of ASPH had significant effects in reducing tumor morphology [24, 27, 28]. Intriguingly, we previously disclosed that targeting ASPH could significantly promote DNA damage response in hepatocellular carcinoma [24]. Thus, we further investigated how ASPH is involved in chemotherapy-associated DNA damage responses. The expression of ASPH partially mitigated DNA damage while the knockdown of ASPH synergistically enhanced DNA damage caused by chemotherapy (Figure 5). This effect was only seen in wild-type ASPH, whereas mutant ASPH did not have this attribute as seen in ASPH variant 3 lacking enzymatic function or domains. With this in mind, we hypothesized that upstream substrates of ASPH can increase ASPH activity and suppress DNA damage when exposed to chemotherapy. While 2-OG can partially suppress DNA damage in a dose-dependent manner when ASPH is insufficient, the overexpression of ASPH almost masks that effect (Figure 6A). Pre-treating ASPH expressing CCA cells, H1, with 2-OG further improved cell growth rate in MTT assay (Figure 6B). This suggests activation of ASPH by substrates, enzymes or a change in cellular condition can also suppress DNA damage. Although targeting upstream ASPH substrates or enzymes might

be an effective therapy for controlling ASPH activity, the consequences of such an approach is too large as the substrates 2-OG and Fe(II) are both essential components in numerous enzymes [34]; thus targeting ASPH directly would be a better alternative, especially since ASPH inhibitors such as MO-I-1151 are already developed and being tested [27, 37].

Previous studies have demonstrated that the inhibition or knockdown of ASPH induced senescence and impaired tumor growth in cancer cells [24, 31]. The administration of MO-I-1151 to EV transfected cells yielded similar outcomes as shASPH transfected cells for senescence and MTT assays [24]. In this study we challenged ASPH knockdown shASPH with DOX and observed a further increase in senescence and decrease in tumor growth (Figure 7). Upon further analysis, shASPH-DMSO had similar efficacy as shLuc-DOX in all 4 assays, suggesting that the presence of ASPH impedes chemotherapy effects. Once ASPH activity is impaired, chemotherapies can be used to greater effect in inducing DNA damage.

ASPH inhibitor MO-I-1151 has been previous described in studies for suppressing ASPH activity [24, 30, 31, 37]. In patients, ASPH expression has been linked to poorer prognoses [10, 11], in fact a Kaplan Meier graph of progression free survival and overall survival clearly shows a separation between patient groups [11, 37]. To test the physiological effects of ASPH in response to chemotherapy we created two xenograft models. In both cases, tumors that expressed ASPH were more resistant to chemotherapy and had tumors that were on average larger, and increased number of

metastases compared low ASPH with DOX. Patient data also observed increased metastasis and tumor size with high ASPH expression [11].

Following the detection of a DSB by MRN and the activation of ATM, H2aX is phosphorylated and assists in the signaling for DNA damage repair [20]. The involvement of ASPH in this process is unclear but ASPH is known bind with H2AX in the mitochondrial DNA replication signaling pathway [20]. We have demonstrated ATM interacts with ASPH and the increased expression of ASPH led to an increase in binding between ATM and MRN when challenged with a DNA damage inducer (Figure 9). This suggests ASPH may undergo a conformational change that induces ATM binding to MRN thus increasing the rate of DNA repair and decreasing the phosphorylation of H2AX. It is also possible ASPH-mediated hydroxylation of ATM will alter the activity or binding affinity of ATM to MRN and promote DNA repair.

ASPH may play an influential role in the DNA damage response. This may explain the clinical observations of patients with high ASPH expression resistance to chemotherapy and shorter overall survival [10, 11, 37]. While an understanding for the role of ASPH in DNA damage repair through ATM has been explored, further investigation into ATR and DNApkcs is required to better picture of how expression of ASPH results in a decrease in γH2aX expression; whether it is due to an inhibition of DNA damage or promotion of DNA damage repair. A combination therapy that targets ASPH with chemotherapy not only significantly increased DNA damage but also stunted tumor growth and induced senescence. These findings suggest that ASPH is a good candidate for a therapeutic target. The second-generation ASPH inhibitor is an effective antitumor

agent when combined with chemotherapy for high ASPH expression tumors by dramatically increasing DNA damage.

Reference

[1] Gavin Low, Edward Leen, Clinical Ultrasound (Third Edition) Volume 1, 2011, Pages 138-166

[2] Kheman Rajkomar, Jonathan B. Koea. Blumgart's Surgery of the Liver, Biliary Tract and Pancreas. Sixth Edition

[3] Alpini, G. , McGill, J. M. and LaRusso, N. F. (2002), The pathobiology of biliary epithelia. Hepatology, 35: 1256-1268. doi:10.1053/jhep.2002.33541

[4] Tyson GL, El-Serag HB. Risk factors for cholangiocarcinoma. Hepatology. 2011;54(1):173-84.

[5] Hammill CW, Wong LL. Intrahepatic cholangiocarcinoma: a malignancy of increasing importance. J Am Coll Surg. 207(4):594-603, 2008

[6] H. Malhi, G.J. Gores. Cholangiocarcinoma: modern advances in understanding a deadly old disease. J Hepatology, 45 (2006), pp. 856-867

[7] Sia et al., 2013. Sia D., Hoshida Y., Villanueva A., Roayaie S., Ferrer J., Tabak B., et al: Integrative molecular analysis of intrahepatic cholangiocarcinoma reveals 2 classes that have different outcomes. Gastroenterology. 2013; 144: pp. 829-840

[8] Wise C, Pilanthananond M, Perry BF, Alpini G, McNeal M, Glaser SS. Mechanisms of biliary carcinogenesis and growth. World J Gastroenterol 2008; 14(19): 2986-2989

[9] Singh P, Patel T. Advances in the diagnosis, evaluation and management of cholangiocarcinoma. CURRENT OPINION IN GASTROENTEROLOGY. 22(3):294-299.

[10] Lavaissiere L, Jia S, Nishiyama M, et al. Overexpression of human aspartyl(asparaginyl)beta-hydroxylase in hepatocellular carcinoma and cholangiocarcinoma. The Journal Of Clinical Investigation. 1996;98(6):1313-1323.

[11] Maeda T, Taguchi K, Aishima S, et al. Clinicopathological correlates of aspartyl(asparaginyl)beta-hydroxylase over-expression in cholangiocarcinoma. CANCER DETECTION AND PREVENTION. 2004;28(5):313-318. doi:10.17/j.cdp.2004.06.001.

[12] Hausinger RP. Fe(II)/α -Ketoglutarate-Dependent Hydroxylases and Related Enzymes. Critical Reviews in Biochemistry & Molecular Biology. 2004;39(1):21-68. doi:10.1080/10409230490440541.

[13] Jia S, VanDusen WJ, Diehl RE, Kohl NE, Dixon RA, Elliston KO, et al. cDNA cloning and expression of bovine aspartyl (asparaginyl) beta-hydroxylase. J Biol Chem 1992;267:14322-14327.

[14] Monkovic, D.D., et al., Invertebrate aspartyl/asparaginyl beta-hydroxylase: potential modification of endogenous epidermal growth factor-like modules. Biochem Biophys Res Commun, 1992. 189(1): p. 233-41.

[15] Jia, S., et al., A fully active catalytic domain of bovine aspartyl (asparaginyl) beta-hydroxylase expressed in Escherichia coli: characterization and evidence for the identification of an active-site region in vertebrate alpha-ketoglutarate-dependent dioxygenases. Proc Natl Acad Sci U S A, 1994. 91(15): p. 7227-31.

[16] Hu, Y.Y., et al., Notch signaling pathway and cancer metastasis. Adv Exp Med Biol, 2012. 727: p. 186-98.

[17] Sekiya, S. and A. Suzuki, Intrahepatic cholangiocarcinoma can arise from Notch-mediated conversion of hepatocytes. J Clin Invest, 2012. 122(11): p. 3914-8.

[18] Imamura, T., A. Hikita, and Y. Inoue, The roles of TGF-beta signaling in carcinogenesis and breast cancer metastasis. Breast Cancer, 2012. 19(2): p. 118-24.

[19] Carethers, J.M., Intersection of transforming growth factor-beta and Wnt signaling pathways in colorectal cancer and metastasis. Gastroenterology, 2009. **137**(1): p. 33-6

[20] Kinner A, Wu W, Staudt C, Iliakis G. Gamma-H2AX in recognition and signaling of DNA double-strand breaks in the context of chromatin. Nucleic Acids Res. 2008;36(17):5678-94.

[21] Campisi J. Cellular senescence as a tumor-suppressor mechanism. Trends Cell Biol 2001;11:S27-S31.

[22] Campisi J, d'Adda di Fagagna F. Cellular senescence: when bad things happen to good cells. Nat Rev Mol Cell Biol 2007;8:729-740.

[23] Hanahan D, Weinberg RA. The hallmarks of cancer. Cell 2000;100:57-70.

[24] Iwagami Y, Huang C-K, Olsen MJ, et al. Aspartate beta-Hydroxylase Modulates Cellular Senescence Through Glycogen Synthase Kinase 3 beta in Hepatocellular Carcinoma. HEPATOLOGY. 63(4):1213-1226. doi:10.3/hep.28411.

[25] Lamarche BJ, Orazio NI, Weitzman MD. The MRN complex in double-strand break repair and telomere maintenance. FEBS Lett. 2010;584(17):3682-95.

[26] Mah, L.J., A. El-Osta, and T.C. Karagiannis, gammaH2AX: a sensitive molecular marker of DNA damage and repair. Leukemia, 2010. 24(4): p. 679-86.

[27] Aihara A, Huang CK, Olsen MJ, Lin Q, Chung W, Tang Q, et al. A cell-surface beta-hydroxylase is a biomarker and therapeutic target for hepatocellular carcinoma. EPATOLOGY 2014;60: 1302-1313.

[28] Dong X, Lin Q, Aihara A, Li Y, Huang CK, Chung W, et al. Aspartate beta-hydroxylase expression promotes a malignant pancreatic cellular phenotype. Oncotarget 2015;6:1231-1248.

[29] Dickey JS, Redon CE, Nakamura AJ, Baird BJ, Sedelnikova OA, Bonner WM. H2AX: functional roles and potential applications. Chromosoma. 2009;118(6):683–692. doi:10.8/s00412-009-0234-4

[30] Hou G, Xu B, Bi Y, et al. Recent advances in research on aspartate β-hydroxylase (ASPH) in pancreatic cancer: A brief update. Bosn J Basic Med Sci. 2018;18(4):297–304. Published . doi:10.17305/bjbms.2018.3539

[31] Huang CK, Iwagami Y, Aihara A, et al. Anti-Tumor Effects of Second Generation β-Hydroxylase Inhibitors on Cholangiocarcinoma Development and Progression. PLoS One. 2016;11(3):e0150336. Published 2016 Mar 8. doi:10.1371/journal.pone.0150336

[32] Patel N, Khan AO, Mansour A, et al. Mutations in ASPH cause facial dysmorphism, lens dislocation, anterior-segment abnormalities, and spontaneous filtering blebs, or Traboulsi syndrome. Am J Hum Genet. 2014;94(5):755–759. doi:10.17/j.ajhg.2014.04.002

[33] Lavaissiere L, Jia S, Nishiyama M, et al. Overexpression of human aspartyl(asparaginyl)beta-hydroxylase in hepatocellular carcinoma and cholangiocarcinoma. J Clin Invest. 1996;98(6):1313–1323. doi:10.1172/JCI118918

[34] Martinez S, Hausinger RP. Catalytic Mechanisms of Fe(II)- and 2-Oxoglutarate-dependent Oxygenases. J Biol Chem. 2015;290(34):20702–20711. doi:10.1074/jbc.R115.648691

[35] Tang C, Hou Y, Wang H, et al. Aspartate β-hydroxylase disrupts mitochondrial DNA stability and function in hepatocellular carcinoma. Oncogenesis. 2017;6(7):e362. Published 2017 Jul 17. doi:10.1038/oncsis.2017.64

[36] Zou Q, Hou Y, Wang H, et al. Hydroxylase Activity of ASPH Promotes Hepatocellular Carcinoma Metastasis Through Epithelial-to-Mesenchymal Transition Pathway. EBioMedicine. 2018;31:287–298. doi:10.17/j.ebiom.2018.05.004

[37] Sturla LM, Tong M, Hebda N, et al. Aspartate-β-hydroxylase (ASPH): A potential therapeutic target in human malignant gliomas. Heliyon. 2016;2(12):e00203. Published 2016 Dec 5. doi:10.17/j.heliyon.2016.e00203